Bose-Hubbard model with occupation-parity couplings

Kuei Sun and C. J. Bolech
Department of Physics, University of Cincinnati, Cincinnati, Ohio 45221-0011, USA
(Received 20 September 2013; revised manuscript received 29 January 2014; published 18 February 2014)

We study a Bose-Hubbard model having on-site repulsion, nearest-neighbor tunneling, and ferromagneticlike coupling between occupation parities of nearest-neighbor sites. For a uniform system in any dimension at zero tunneling, we obtain an exact phase diagram characterized by Mott-insulator (MI) and pair liquid phases and regions of phase separation of two MIs. For a general trapped system in one and two dimensions with finite tunneling, we perform quantum Monte Carlo and Gutzwiller mean-field calculations, both of which show the evolution of the system, as the parity coupling increases, from a superfluid to wedding-cake-structure MIs with their occupations jumping by 2. We also identify an exotic pair superfluid at relatively large tunneling strength. Our model ought to effectively describe recent findings in imbalanced Fermi gases in two-dimensional optical lattices and also potentially apply to an anisotropic version of bilinear-biquadratic spin systems.

DOI: 10.1103/PhysRevB.89.064506 PACS number(s): 67.85.Hj, 67.85.Lm, 05.30.Rt, 75.10.Jm

I. INTRODUCTION

Since half a century ago, the Hubbard model has been widely studied as a simple model accounting for several nontrivial phenomena in electronic systems, such as the Mott insulator, (anti)ferromagnetism, and novel superconductivity [1–5]. Its bosonic version, the Bose-Hubbard (BH) model, has been appreciably investigated for more than two decades [6,7]. The BH model not only aptly describes the many-body behavior of bosons in lattices, but also serves as a good and simple example for understanding how competition between two common mechanisms, localization and itineracy, can drive matter toward extremely different phases, namely Mott-insulator (MI) or superfluid. The MI phase, characterized by commensurate occupations, gapped excitations, and incompressibility, undergoes a transition to a superfluid, characterized by Bose-Einstein condensation, gapless excitations, and finite compressibility, as the ratio of tunneling to interaction energy increases beyond a density-dependent critical value. Differently from the fermionic case, the bosonic nature allows the BH phase diagram of multiple MI regions for all possible integer occupations, surrounded by the superfluid region. Various realizations of the BH model have been early suggested in granular systems with an embedded condensate, such as a Josephson junction array [8,9] or liquid helium in porous media [10,11], and later in lattice bosons, such as bosonic atoms in optical lattices [12] or exciton polaritons in an array of microcavities [13–16]. Recent achievements in cold-atom experiments have successfully created inhomogeneous BH systems and realized the MI-superfluid transition [17] as well as a spatially separated structure of multiple MIs [18]. These multiple applications have stimulated a broad interest in the BH physics and lead to an active study of a great variety of BH models [19–23].

Recently, a theoretical investigation we carried out on imbalanced fermionic superfluids in a two-dimensional (2D) array of coupled tubes [24] [a setup which has been experimentally realized [25] in the search for the elusive Fulde-Ferrell-Larkin-Ovchinnikov (FFLO) state [26–29]] has shown an exotic compressible-incompressible quantum phase transition of the tube occupation of unpaired majority fermions (UMFs) in the system. The phase diagram obtained from the microscopic model of fermions exhibits similarities and contrasts to the structure as a BH phase diagram. On the one hand there is a phase with well defined UMF occupation numbers in each tube. On the other hand, the occupations of the incompressible (MI) regions are either all even or all odd. The similarities reflect the competition between the on-tube energy and cross-tube kinetics of the UMFs and hence suggests an effective description of the (projected) system by a 2D BH model, while the contrasts suggest the need for an additional term in the effective model that "orients" the occupation parities (see Sec. II below for a detailed discussion).

Motivated by this previous work, we study an extended BH model having a ferromagneticlike coupling between occupation parities of nearest-neighbor sites. This proposed coupling can be pictured as domain-wall energies between nearest-neighbor sites of opposite occupation parities, reminiscent of local magnetization kinks in the ferromagnetic Ising model [7], resulting in a ground state that favors all the sites having the same occupation parity. The parity coupling shows interesting interplays with the other two original BH ingredients, single-particle tunneling, and on-site repulsion. First, it is antagonistic toward the single-particle tunneling process, during which two involved neighbor sites flip the parity and form domain walls between themselves and the surrounding sites [see illustration in Figs. 1(a) and 1(b)]. Second, it is different from the on-site repulsion in that it drives the system to accept additional doping as pairs rather than single particles, to avoid the domain-wall energy, while the on-site repulsion does the opposite as a way to reduce the interaction energy [see Figs. 1(c) and 1(d)]. In this paper, we analyze the system and characterize the effects of the occupation-parity coupling. We will suggest two possible experimental realizations for exploring the model in cold atomic and condensed-matter systems. We shall find a rich phase diagram for the uniform case in the zero-tunneling limit, reflecting different doping preferences driven by the parity coupling and on-site repulsion. For the finite-tunneling case, we apply two commonly used treatments, quantum Monte Carlo [30–33] (QMC) and Gutzwiller mean-field [34] (GMF) methods, on trapped systems, thus successfully describing the state of the system as the parity coupling increases for finite tunneling. In the large-tunneling regime, we identify an exotic pair superfluid state, which emerges with a different mechanism from previously studied ones [35–41].

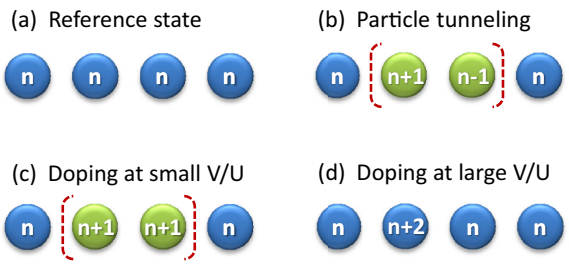

FIG. 1. (Color online) Illustration of the energetic competition between particle tunneling t, interaction U, and parity coupling V of the system. (a) A reference state of each site occupied by n particles. (b) After a single-particle tunneling, the change in number of two neighbor sites alters the interaction energy by $O(U)$, while the change in parity of them results in a domain-wall formation (dashed curve) of energy cost $O(V)$. (c) At small V/U, two doping particles tend to occupy different sites, minimizing the interaction energy. (d) At large V/U, the two occupy the same site as a pair doping, avoiding the domain-wall energy.

The paper outline is as follows. In Sec. II, we introduce the model Hamiltonian and discuss its possible realizations by studying its emergence in imbalance Fermi gases as well as in spin systems. In Sec. III, we perform a detailed analysis of the competition between the parity coupling and the on-site repulsion, and obtain an exact phase diagram in the zero-tunneling plane. In Sec. IV, we present results from QMC and GMF calculations that show the evolution of a trapped system and the emergence of the pair superfluid. Finally, we summarize our work in Sec. V.

II. MODEL

The extended BH model with occupation-parity couplings between nearest-neighbor sites is described by the Hamiltonian

$$H = \sum_{\langle ij\rangle} -t(\hat{b}_i^\dagger \hat{b}_j + \text{H.c.}) - \frac{V}{2}(\hat{P}_i \hat{P}_j - 1) + \sum_i \frac{U}{2}\hat{n}_i(\hat{n}_i - 1) - \mu_i \hat{n}_i, \quad (1)$$

where $\hat{b}_i$ is a bosonic operator on site i, $\hat{n}_i = \hat{b}_i^\dagger \hat{b}_i$ is the number operator, $\hat{P}_i = (-1)^{\hat{n}_i}$ is the number-parity operator, μ_i is the local chemical potential, and $\langle ij\rangle$ denotes a pair of neighboring sites. The non-negative parameters t, V, and U give the strength of nearest-neighbor tunneling, ferromagnetiklike nearest-neighbor parity coupling, and on-site repulsion, respectively. Each pair of them show a competition that is reflected in the ground state of the system. At $V = 0$, the Hamiltonian returns to the original BH one, in which the domination of itineracy (large t/U) or localization (large U/t) results in a superfluid or MI, respectively. The presence of V terms can be regarded as an energy cost of domain walls between two neighboring sites with different number parities. From this point of view, the competition between t and V can be described by the picture that a single-particle tunneling changes the parities of two sites and hence pays an energy cost of creating a domain wall surrounding them [see Figs. 1(a) and 1(b)]. Therefore, when V dominates, the system favors the minimization of the total number of domain walls, that is, to have all sites with the same occupation parity. The interplay between U and V yields a rich phase diagram, which will be discussed in detail in Sec. III. Here, we now turn to discuss two possible realizations of our model.

First, a recent study in Ref. [24] has suggested that the mechanism in the Hamiltonian of Eq. (1) accounts for an exotic quantum phase transition in imbalanced fermionic superfluids in optical lattices. The system has the geometry of a 2D array composed of one-dimensional (1D) tubes that has been realized in experiments [25,42,43]. In such a system it is the behavior of spin imbalance per tube, or the fillings of UMFs, that undergoes a transition from a compressible state (UMF move easily across tubes) to a MI (UMFs are localized on each tube), yielding a similar phase diagram to the regular BH one except the filling numbers of the MI phases are either all even or all odd while they can be any integer in the regular case. Regarding the projection of this anisotropic three-dimensional fermionic system to an effective 2D lattice model described by Eq. (1), we find the tunneling t and on-site interaction U as a result from the interplay of the lattice geometry, on-tube interaction, and on-tube pairing order. The occupation-parity coupling V comes from the domain-wall energy between two neighboring tubes having different spatial parities of the oscillatory superconducting order parameter, which is directly related to the occupation parity of UMFs. In the Appendix A, we present a detailed derivation showing how the physics of UMFs is effectively described by Eq. (1), by starting from the original Hamiltonian of the fermionic superfluid system. We remark that the parameter regimes discussed in Ref. [24] are for the large V limit. However, the high tunability of lattice geometry and interatomic interaction in this cold atomic system could enable the exploration of sufficiently wide parameter regimes of our model Hamiltonian.

Second, the regular BH model can be mapped to a spin-1 ($\hat{\mathbf{S}}$) system around the tip of the Mott insulator lobe in the large-occupation limit, in which a three-state truncation applies on each site [44]. For our model, the occupation parity coupling terms are mapped to spin couplings of the Ising-type with quadratic and biquadratic forms. Taking the truncation basis of integer occupation states $|n\rangle$ and $|n \pm 1\rangle$, we perform the mapping $\hat{b}^\dagger \to \sqrt{n}\hat{S}^+$, $\hat{n} \to n + \hat{S}^z$, as well as $\hat{P} \to (-1)^n[1 - 2(\hat{S}^z)^2]$ on Eq. (1) and obtain a spin Hamiltonian,

$$H_S = \sum_{\langle ij\rangle} -J_1(\hat{S}_i^x \hat{S}_j^x + \hat{S}_i^y \hat{S}_j^y) - J_2(\hat{S}_i^z)^2(\hat{S}_j^z)^2 + \sum_i D(\hat{S}_i^z)^2 + h_i \hat{S}_i^z, \quad (2)$$

up to a constant offset. Here $J_1 = 2nt$, $J_2 = 2V$, $D = ZV + U/2$ with Z being the coordination number and $h_i = (n - 1/2)U - \mu_i$. One immediately sees the competitions in Eq. (2): the bilinear coupling J_1 aligns spins in the x-y plane, the biquadratic coupling J_2 drives spins to $S^z = \pm 1$ states, the nonlinear Zeeman coupling D drives them to $S^z = 0$ state, and the local magnetic field h_i aligns them in the z direction. The first line in Eq. (2) can be regarded as an anisotropic version of standard bilinear-biquadratic spin models [45–51], whose

experimental realization has been discussed in condensed matter [52] and cold atomic gases [53,54]. The second line commonly appears in nonlinear spin systems [55–57]. A recent study on fermionic dipolar gases [58] also found a route toward the creation of an anisotropic spin system, as a variant of Eq. (2). Due to the connection between the two models, the realization of the spin system could provide an alternative approach for examining a variant of our model bosonic system, and vice versa.

III. PHASE DIAGRAM AT $t = 0$

In this section we discuss the competition between the on-site interaction U and the parity coupling V through additional doping of a uniform system in the zero-tunneling regime. We derive exact energy functionals in any dimension for each competing phase and obtain the ground-state phase diagram marking their relatively energetically favorable regions.

At $t = 0$, the ground state is a product of each single-site state with integer occupation n_i on site i. The configuration of $\{n_i\}$ is obtained by minimizing the system's energy. At integer fillings n, we have a MI with all $n_i = n$ [Fig. 1(a)], independent of the ratio V/U. Now considering the doping of two additional particles in the system, if U dominates (small V/U), we expect that the two particles will occupy different sites to avoid higher interaction energy [Fig. 1(c)]. Such two sites with $n + 1$ occupation can be arbitrary ones at $V = 0$ and should bind together as neighbors at $V > 0$ due to the *domain-wall* effect. For more than two particles added, they similarly tend to singly dope sites that randomly spread if $V = 0$ or cluster if $V > 0$. We call the former case a single-particle doped liquid (SL) and the latter a phase separation of two MIs (PS). If V dominates (large V/U), to avoid the domain-wall energies, the two doping particles tend to occupy the same site producing pair doping [Fig. 1(d)], thus keeping the parity of all sites unchanged. More than two particles will doubly dope in the same way, up to one doping pair per site due to the interaction effects. We call such state a pair-doped liquid (PL). Similarly, when particles are taken out of the system (in analogy to the hole doping in fermionic systems), they leave as single particles at large U and as on-site pairs at large V. Below we calculate the phase boundary between PS and PL in a homogeneous system.

In the case of doping $M_\pm$ particles (holes) in a d-dimensional uniform system of L^d sites with integer filling n ($M_\pm$ is taken even and $M \leqslant L^d/2$), the PS state has $M_\pm$ sites of $n \pm 1$ filling, $L - M_\pm$ sites of n filling, and $N_{\rm DW}$ domain-wall links, while the PL state has $M_\pm/2$ sites of $n \pm 2$ filling, $L - M_\pm/2$ sites of n filling, and no domain walls. The energies of the PS and PL states can thus be written as

$$E_{\rm PS}(n, M_\pm) = M_\pm E_U(n \pm 1) + (L^d - M_\pm)E_U(n) + N_{\rm DW}V, \quad (3)$$

and

$$E_{\rm PL}(n, M_\pm) = \frac{M_\pm}{2}E_U(n \pm 2) + \left(L^d - \frac{M_\pm}{2}\right)E_U(n), \quad (4)$$

respectively, where $E_U(n) = Un(n-1)/2$ is the on-site interaction energy. We let $E_{\rm PS} = E_{\rm PL}$ to obtain a critical ratio $(V/U)_c$ that the separates PS and PL states,

$$\left(\frac{V}{U}\right)_c = \frac{M_\pm}{2N_{\rm DW}}. \quad (5)$$

Given periodic boundary conditions for the system, the doped domain favors a spherical shape to minimize the surface area or the number of domain-wall links, so we have $M_\pm = \tau_d R^d$ and $N_{\rm DW} = s_d R^{d-1}$, where R is the domain radius and τ_d (s_d) is the volume (surface area) of a d-dimensional unit sphere. Substituting these relations in Eq. (5) and rewriting the doping in terms of a rescaled coupling $\tilde{V} = V/(UL)$ and the average filling $\bar{n}$ such that $M_\pm = |\bar{n} - n|L^d$, we obtain

$$\tilde{V}_c = A_d|\bar{n} - n|^{1/d}, \quad (6)$$

where $A_d = (\tau_d)^{(1-1/d)}/(2s_d)$. Equation (6) for $\bar{n} - n < 1/2$ (respectively, $-1/2 < \bar{n} - n$) describes the PS-PL transition due to particle (hole) doping on the n-filling MI, except for $0 < \bar{n} < 1$ when there is no PL that is hole doped from the $n = 1$ MI, so the phases are determined only by particle doping on the vacuum state, where $\tilde{V}_c = A_d\bar{n}^{1/d}$.

Figure 2 shows a combined phase diagram of the $V = 0$ ($\bar{n}$–$\tilde{t}$ plane, where $\tilde{t} = t/U$) and $t = 0$ ($\bar{n}$–$\tilde{V}$ plane) cases in one and two dimensions. At $V = 0$, the system turns to the original BH model: the ground state is a MI (solid section lines) at integer fillings and $\tilde{t}$ below a critical value $\tilde{t}^*$ or is a superfluid (SF) at any fractional filling. Here $\tilde{t}^*$ monotonically increases with dimension d and decreases with filling n. At

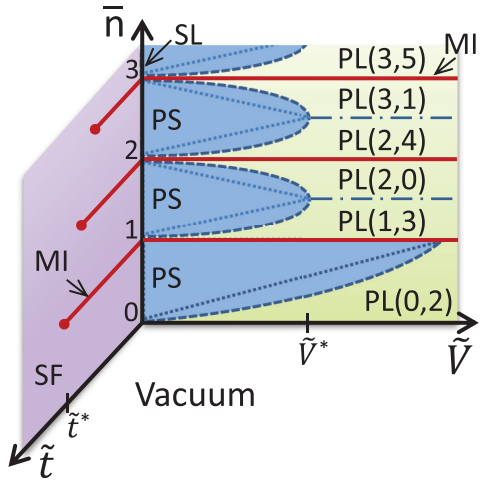

FIG. 2. (Color online) Schematic phase diagram combining $V = 0$ and $t = 0$ cases. Here $\tilde{t} = t/U$ and $\tilde{V} = V/UL$ with L^d being the volume of the system (in d dimensions). In the $V = 0$ plane, the system is a Mott insulator (MI, solid section line) at integer fillings and $\tilde{t} \leqslant \tilde{t}^*(d,n)$ or is a superfluid (SF) otherwise. In the $t = 0$ plane, the system is MI (solid line) at integer fillings and any V. At any fractional filling and finite V, the system is phase separated into two MIs (PS), or is a pair-doped liquid (PL), distinguished by the critical relation in Eq. (6) [dashed (dotted) curve in two (one) dimensions]. In the PL regime at $1 \leqslant n < \bar{n} < n + 1$, the half integer fillings (dash-dotted curve) separate two types of PL of different parities, PL(n,$n + 2$) as well as PL($n + 1$,$n - 1$), and meet the PS lobe at a "triple point" $\tilde{V}^*(d)$ (see text for more details). In the $\bar{n}$ axis, the fractional-filling region is a single-particle doped liquid (SL).

$t = 0$, the integer fillings are always MIs (the solid lines extend to $V \to \infty$), while at fractional fillings there are lobelike PS regions (having n and $n+1$ MIs spatially separated given $n < \bar{n} < n+1$) at small $\tilde{V}$, and PL regions outside the lobes. In the PL case, when $\bar{n} > 1$ and goes across half integers (dash-dotted line), the ground state suddenly switches to another subspace of opposite parity and occupations, from a PL being particle doped from the n-filling MI to one being hole doped from the $(n+1)$-filling MI [denoted as PL(n,$n+2$) and PL($n+1$,$n-1$), respectively]. (This continuity in density but discontinuity in parity could invalidate the local-density approximation, which is commonly used to profile a trapped system from the uniform phase diagram [59].) Such parity boundary meets the tip of the PS lobes at a triple point $\tilde{V}^* = A_d 2^{-1/d}$, which is a function of dimension but independent of filling. At $\bar{n} < 1$, there is no such triple point due to the lack of hole-doped PL from the $n = 1$ MI. The PL here is always of even parity [PL(0,2)].

The scaling $\tilde{V} = V/(UL)$ indicates that the PL will eventually disappear in the limit of $L \to \infty$, except in the free case ($U = 0$) when it is the PS state instead of the PL one that disappears. On the other hand, the PL phase is always allowed in a finite-sized or a trapped system and will exist at the interphase between different MI plateaus as will be discussed below. In addition, the rich structure in the $\bar{n}$–$\tilde{V}$ diagram implies a nontrivial interplay when all t, U, and V are nonzero. In Sec. IV, we numerically study and present results for a general trapped system using quantum Monte Carlo and Gutzwiller mean-field methods.

IV. NUMERICAL SIMULATIONS ($t \neq 0$)

In this section we apply two commonly used methods to do calculations for a trapped system (a natural setup in cold-atom experiments), at various values of the parity coupling in one and two dimensions. In a harmonic trap, the system has a local chemical potential of the form

$$\mu_i = \mu_0 - \frac{K}{2}\mathbf{r}_i^2, \tag{7}$$

where μ_0 is the global chemical potential, K is the trap's curvature, and $\mathbf{r}_i$ is the position of site i from the trap center.

First, we use the quantum Monte Carlo (QMC) method and, in particular, the stochastic series expansion (SSE) algorithm [30–33], which has been successfully applied on a variety of BH model studies [60]. We plot the density profile $\rho = \langle \hat{n} \rangle$ from the trap center in 1D lattices [Fig. 3(a)] and that along the diagonal of 2D square lattices [Fig. 3(b)] at a given t that makes the system a superfluid when $V = 0$. In the original BH case ($V = 0$), the superfluid's density profile monotonically and smoothly decreases to zero from the center to the edge (solid curve), matching the shape of the trap. In both the 1D and 2D cases, with an increase in V, the system first develops small MI plateaus at lower integer fillings $\rho = 1,2$ (dashed curves), and then the $\rho = 1$ one disappears while the $\rho = 2$ one expands, as well as higher integer plateaus $\rho = 3,4$ develop (dotted curve). Finally only the even-integer MI plateaus $\rho = 2,4$ survive at large V (dot-dashed curve). The first development of the integer plateaus is because a local domain with integer occupation costs less parity energy than

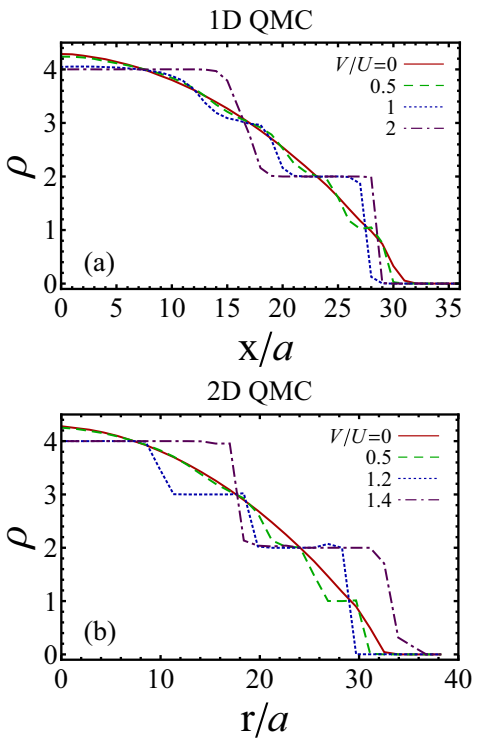

FIG. 3. (Color online) Density profiles ρ obtained from the quantum Monte Carlo (QMC) method at various V. (a) One-dimensional (1D) profiles from the trap center to the edge, at $V/U = 0$, 0.5, 1, and 2. The model parameters are $t/U = 0.2$, $\mu_0/U = 3.5$, $K/U = 0.0075/a^2$, where a is the lattice spacing, and the temperature $T/U = 0.002$. (b) Two-dimensional (2D) profiles along the diagonal of a square lattice, from the trap center to the edge at $V/U = 0$, 0.5, 1.2, and 1.4. The model parameters are $t/U = 0.1$, $\mu_0/U = 3.5$, $K/U = 0.0066/a^2$, and $T/U = 0.002$. In both panels the data are presented in solid, dashed, dotted, and dot-dashed curves respectively for increasing V.

that with fractional one, while the later survival of only the even plateaus is attributable to a boundary behavior, minimizing the interphase energy between plateaus, plus the fact that the density always decreases to zero (even parity) at the edge of the system. We notice that the 2D profile exhibits a rotational symmetry, so at large V it does look like a "wedding cake" but with the adjacent MI plateaus differing by two units.

To compare with the QMC results, we use a Gutzwiller mean-field (GMF) method [34] that has also been widely applied to a variety of lattice-boson systems [61]. The key assumption of the GMF method is to treat the ground state of the system as a variational product of all single-site states,

$$|\psi_g^{\mathrm{GMF}}\rangle = \prod_i \left[\sum_{n=0}^{n_m} f_{i,n} \frac{(b_i^\dagger)^n}{\sqrt{n!}} \right] |\mathrm{vac}\rangle, \tag{8}$$

where n_m is the upper bound of site occupation, $f_{i,n}$ is the amplitude of n occupation on site i, and $|\mathrm{vac}\rangle$ denotes the vacuum state. We obtain the solutions of $\{f_{i,n}\}$ by minimizing the energy functional $\langle \psi_g^{\mathrm{GMF}} | H | \psi_g^{\mathrm{GMF}} \rangle$, subject to the normalization constraint $\sum_{n=0}^{n_m} |f_{i,n}|^2 = 1$. Here n_m is chosen large enough such that we observe convergence of the lowest energy state within the Gutzwiller assumption.

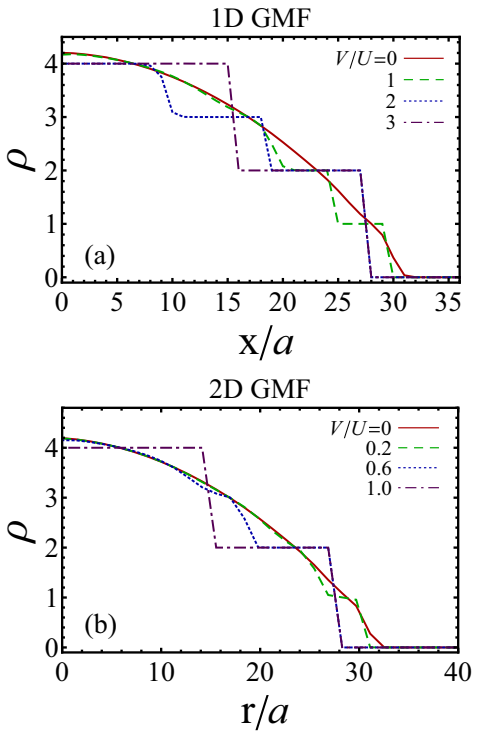

FIG. 4. (Color online) Density profiles obtained from the Gutzwiller mean-field (GMF) method. (a) 1D profiles at $V/U = 0$, 1, 2, and 3. (b) 2D diagonal profiles at $V/U = 0$, 0.2, 0.6, and 1. Data are presented in the same convention as in Fig. 3 and the model parameters are also the same except for $T = 0$.

Figures 4(a) and 4(b) show 1D and 2D density profiles obtained from GMF, respectively. We see the same four-stage evolution from the superfluid to the wedding-cake structure of even-occupation MIs, qualitatively in agreement with the QMC results.

In addition, we investigate a 2D case with larger t, in which the system is always a superfluid ($\langle\hat{b}\rangle \neq 0$ everywhere as long as $\rho \neq 0$) in a range of V of interest. We find that with the increase in V, the outer superfluid shell develops a strong parity *preference*, $\langle\hat{P}\rangle \to \pm 1$, while the inner superfluid core remains the same state ($|\langle\hat{P}\rangle| \ll 1$) as in the $V = 0$ case. This parity preference indicates a pair-doped nature analogous to the PL state in the $t \to 0$ limit (discussed in Sec. III), while the concurrence of the superfluid order suggests the itineracy of particles as pairs, reminiscent of pair superfluids in multispecies lattice bosons [35–37] or dimer superfluids in BH systems with attractive interactions [38–41]. We identify such a pair-superfluid state by a combined order parameter,

$$\psi_P = |\langle\hat{b}\rangle|^2\langle\hat{P}\rangle. \tag{9}$$

Notice that the sign of ψ_P tells the pair superfluid's parity being even (+) or odd (−).

In Fig. 5 we plot profiles of ψ_P [5(a)] and ρ [5(b)] obtained from GMF calculations at a set of increasing V values and t five times larger than that in Fig. 4(b). At $V = 0$, ψ_P shows no parity preference in the central region, due to a smooth occupation distribution $|f_n|^2$, and slowly alternates between positive (even) and negative (odd) when the density becomes dilute near the edge (because the occupation amplitudes $\{f_{i,n}\}$

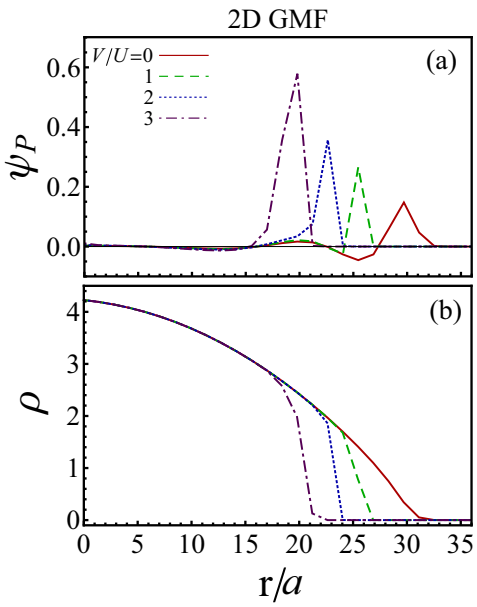

FIG. 5. (Color online) (a) Pair-superfluid order ψ_P and (b) the corresponding density profile along the diagonal in 2D trapped lattices at $V/U = 0$, 1, 2, and 3 (solid, dashed, dotted, and dot-dashed curves respectively). Data are obtained using GMF with the model parameters being $t/U = 0.5$, $\mu_0/U = 2.5$, $K/U = 0.0066/a^2$, and $T = 0$.

are asymmetrically distributed in n, with a natural cutoff by $n = 0$). As V increases, ψ_P develops a strong preference of even parity in the outer shell region (pair superfluid), leaving the inner core still parity undefined (regular superfluid). We see that the density of the outer shell drops much faster when it becomes a pair superfluid, indicating that the pair superfluid has higher compressibility ($\partial\rho/\partial\mu$) than the regular superfluid. We point out that the pair superfluid here results from the co-tunneling of two particles to avoid the flipping of site's occupation parities. The mechanism is different from the pair superfluids in other systems [35–41], in which two particles are directly bound by attractive interactions.

V. CONCLUSION

In this paper, we studied an extended Bose-Hubbard model incorporating a ferromagneticlike coupling between the nearest-neighbor site-occupation parities. This parity coupling generates domain-wall energies that compete with the single-particle tunneling and favors pair doping rather than the single-particle one that is favored instead by the on-site repulsion. The interplay between the parity coupling and on-site repulsion leads to a rich phase diagram of a uniform system at zero tunneling, characterized by (1) Mott-insulator (MI) phases at each commensurate filling and (2) phase separation of two MIs when the on-site interaction dominates or (3) pair-liquid phases when the parity coupling dominates at incommensurate fillings. In the finite-tunneling inhomogeneous case, we have obtained both quantum Monte Carlo and Gutzwiller mean-field results that agreeably show an evolution of a trapped system from a superfluid to a wedding-cake structure of MIs with the same parity (or the occupation jumping by 2), as the parity coupling increases. In a relatively large tunneling and

large-parity coupling regime, the trapped system exhibits a structure with the inner bulk being a single-particle superfluid as usual and the outer shell being an exotic pair superfluid.

Considering the realization of our model, we have shown that it effectively describes the behavior of the UMFs in a system of imbalanced fermionic superfluids in 2D optical lattices of tubes, which has been realized [25] and is being studied in ongoing experiments [62]. The transition between a superfluid and MIs of the same parity in our model corresponds to that between compressible and incompressible states of UMFs in the tubular system with a strong oscillatory pairing order [24]. Such transition can be detected by the response of the UMFs to optical-lattice modulation [63,64] or by the momentum distribution of UMFs in a time-of-flight experiment [65–68]. The pair-superfluid state in our model corresponds to the compressible state of itinerant UMF pairs in the tubular system, reminiscent of a triplet-pair superfluid. In addition, a truncated version of our model can be mapped to an anisotropic bilinear-biquadratic spin model, in which the occupation-parity coupling is associated with biquadratic spin coupling. Such mapping provides a potential realization for exploring our model in spin systems and would also stimulate interest in the physics of these two models.

ACKNOWLEDGMENTS

We are grateful to R. G. Hulet, M. Ma, and M. Troyer for useful discussions. The QMC calculations have been performed using the SSE algorithm provided by the ALPS project [31–33]. This work was supported by DARPA-ARO Award No. W911NF-07-1-0464 and by the University of Cincinnati. Furthermore, C.J.B. would like to acknowledge the hospitality of the Aspen Center for Physics, supported by the NSF under Grant No. PHYS-1066293.

APPENDIX: DERIVING THE MODEL HAMILTONIAN FROM IMBALANCED FERMIONIC SUPERFLUIDS IN OPTICAL LATTICES

In this Appendix we derive the Hamiltonian of Eq. (1) as an effective model describing the behavior of UMFs in a system of an imbalanced fermionic superfluid in a 2D optical lattice of 1D tubes. The Hamiltonian of the tube system comprises three parts [24,69],

$$H_0 = \int_z \sum_{\mathbf{r},\sigma} \hat{\psi}^\dagger_{\sigma\mathbf{r}}(z)\left(-\frac{\hbar^2\partial_z^2}{2m} + U_{\sigma\mathbf{r}}(z) - \mu_\sigma(z)\right)\hat{\psi}_{\sigma\mathbf{r}}(z), \tag{A1}$$

$$H_1 = \int_z \Delta_{\mathbf{r}}(z)\hat{\psi}^\dagger_{\uparrow\mathbf{r}}(z)\hat{\psi}^\dagger_{\downarrow\mathbf{r}}(z) + \text{H.c.}, \tag{A2}$$

$$H_2 = \int_z \sum_{\langle\mathbf{r}\mathbf{r}'\rangle,\sigma} \mathcal{T}_{\mathbf{r}\mathbf{r}'\sigma}(z)\hat{\psi}^\dagger_{\sigma\mathbf{r}'}(z)\hat{\psi}_{\sigma\mathbf{r}}(z), \tag{A3}$$

where the $\hat{z}$ direction is along the tubes' axis and $\mathbf{r} = (x,y)$ denotes tubes indexed in the lattice plane perpendicular to $\hat{z}$. The operator $\hat{\psi}^\dagger_{\sigma=\uparrow/\downarrow,\mathbf{r}}(z)$ creates a majority (minority) spin at position z on tube $\mathbf{r}$. The first part H_0 contains the kinetic energy in the $\hat{z}$ direction, the Hartree field U and the spin-dependent chemical potential μ (we assume homogeneity in the $\hat{\mathbf{r}}$ direction), the second part H_1 includes the superfluid pairing order Δ, while the third part H_2 models the tunneling between nearest-neighbor tubes $\langle\mathbf{r}\mathbf{r}'\rangle$. The tunneling field $\mathcal{T}$ describes the effective single-particle tunneling under the influence of the pairing state of the surrounding tubes [69]. The three coupling fields U, Δ, and $\mathcal{T}$ are introduced after employing a Bogoliubove–de Gennes (BdG) treatment [70] on the original Hamiltonian of a quartic form; which includes, besides the single-particle Hamiltonian, a two-body point-contact interaction and (possible) pair tunneling. The Hamiltonian $H_0 + H_1 + H_2$ can be solved in a quasiparticle basis, resulting in a set of $\{U,\Delta,\mathcal{T}\}$ that self-consistently describes the equilibrium state of the system (see detailed discussions in Refs. [24] and [69] as well as a wide application of this treatment on similar systems [71–75]).

The self-consistent solutions show that in the presence of spin imbalance, the system can accommodate an oscillatory pairing order Δ along the tube axis (the FFLO state [26–29]). For a single tube or uncoupled tubes, each UMF is localized around a node of the pairing order parameter such that the total numbers of nodes and UMFs are equal. Given the spatially symmetric confinement along the tube axis, e.g., a harmonic trap, a tube with odd (even) imbalance has a pairing node (antinode) at the tube center. In particular, the localized UMFs can be regarded as occupied Andreev bound states [72,76], resulting in an imbalance profile like separated solitons [77,78] if the spatial distribution of the pairing nodes is relatively sparse or like a ripple [73] if it is dense. (The same signatures have also been found in isotropic three-dimensional Hubbard lattices [79] or coupled Hubbard chains [80].) Both configurations arise from the same effect of localization and can be characterized as the spatial concurrence of imbalance peaks and pairing nodes.

The localization of UMFs suppresses the degrees of freedom in the $\hat{z}$ direction and hence allows us to construct an effective 2D lattice model describing the physics of UMFs with only the $\hat{\mathbf{r}}$ degree of freedom. We remark that even if UMFs localize along the $\hat{z}$ direction, they can still be mobile in the $\hat{\mathbf{r}}$ direction, constituting the physics of interests as discussed below. In such a 2D model the state in the $\hat{z}$ direction is taken as a hidden degree of freedom of a lattice site. (This idea has also been applied on bosonic gases in tubular lattices [81–85], in which the multiorbital wave functions in the tube direction are incorporated into on-site degrees of freedom for an effective 2D model across the tubes.) The hidden degrees of freedom here can be directly related in one-to-one correspondence to the site occupation number, and since more than single occupation per site are possible, this suggests a bosonic description for the modeling. Formally, one can still keep the anticommutation relation in the $\hat{\mathbf{r}}$ direction by using a combined operator

$$\psi_{\uparrow\mathbf{r}}(z) \to \hat{\eta}_{\mathbf{r}}\hat{b}_{\mathbf{r}}, \tag{A4}$$

where $\hat{b}$ is a bosonic operator accounting for occupation-related physics and $\hat{\eta}$ is a Majorana fermion operator carrying the statistical property of the original fermions. Based on this decoupling, we build our model step by step below.

First, for coupled tubes, the pairing nodes tend to line up at the same z positions on each tube [24,69]. The leading kinetics across the tubes is the transverse tunneling of an UMF from a pairing node in a tube to the corresponding one in the nearest neighbor. The one-particle tunneling of minority fermions is suppressed provided they are all paired (at low temperature). Because a node is surrounded by other nodes where the pairing is zero, the tunneling field reduces to a free particle tunneling strength [69], $\mathcal{T} \to -t$. Therefore, considering the order-parameter configuration in H_1 that limits the kinetics in H_2 to be only for the UMFs, we obtain the tunneling term in the model as

$$-t\sum_{\langle \mathbf{r}\mathbf{r}'\rangle}\psi^{\dagger}_{\uparrow\mathbf{r}'}\psi_{\uparrow\mathbf{r}} \to -t\sum_{\langle \mathbf{r}\mathbf{r}'\rangle}\hat{b}^{\dagger}_{\mathbf{r}'}\hat{\eta}_{\mathbf{r}'}\hat{\eta}_{\mathbf{r}}\hat{b}_{\mathbf{r}}. \tag{A5}$$

Second, if the coupling between the tubes is weak enough, the on-site energy is mainly contributed by the on-tube kinetics, Hartree energy, pairing energy, and chemical potentials, all of which are determined once the on-site filling (of UMFs) is given. The self-consistent calculation in Ref. [24] shows that the on-site energy is nonlinear and can be fitted by a repulsive interaction U plus a chemical potential μ. As a result, the on-tube energies H_0 and H_1 effectively become the on-site terms of our model as

$$\sum_{\mathbf{r}}\frac{U}{2}\hat{n}_{\mathbf{r}}(\hat{n}_{\mathbf{r}}-1)-\mu\hat{n}_{\mathbf{r}}, \tag{A6}$$

where $\hat{n}_{\mathbf{r}} = \hat{b}^{\dagger}_{\mathbf{r}}\hat{\eta}_{\mathbf{r}}\hat{\eta}_{\mathbf{r}}\hat{b}_{\mathbf{r}} = \hat{b}^{\dagger}_{\mathbf{r}}\hat{b}_{\mathbf{r}}$.

Third, the BdG calculations show that the system energy rises if two nearest-neighbor tubes have different spatial parities of the oscillatory pairing order parameter. Such energy increase comes from a drastic mismatch in the order parameters and can be regarded as a cost of domain-wall formation, exhibiting similar physics to that in superconducting π junctions [86] or weakly imbalanced cold atomic gases [76]. Because the spatial parity of the order parameter is equal to the occupation parity of the UMFs, one can describe the domain-wall physics with the occupation-parity coupling between nearest-neighbor sites in the BH model,

$$-\frac{V}{2}\sum_{\langle \mathbf{r}\mathbf{r}'\rangle}(\hat{P}_{\mathbf{r}'}\hat{P}_{\mathbf{r}}-1), \tag{A7}$$

where $\hat{P}_{\mathbf{r}} = (-1)^{\hat{n}_{\mathbf{r}}}$ is the on-site parity operator and V is the unit-length energy of domain walls.

Finally, by collecting all terms in Eqs. (A5)–(A7) we obtain an effective Hamiltonian,

$$\sum_{\langle \mathbf{r}\mathbf{r}'\rangle}\left[-t(\hat{b}^{\dagger}_{\mathbf{r}'}\hat{\eta}_{\mathbf{r}'}\hat{\eta}_{\mathbf{r}}\hat{b}_{\mathbf{r}}+\text{H.c.})-\frac{V}{2}(\hat{P}_{\mathbf{r}'}\hat{P}_{\mathbf{r}}-1)\right] + \sum_{\mathbf{r}}\left[\frac{U}{2}\hat{n}_{\mathbf{r}}(\hat{n}_{\mathbf{r}}-1)-\mu\hat{n}_{\mathbf{r}}\right]. \tag{A8}$$

Because the physical quantities of interest to be addressed here can be expressed as local static (or equal-time) correlations of the ground state, not involving the exchange of particles, the statistics (Majorana sector) factors out. Therefore, by replacing $\hat{b}^{\dagger}_{\mathbf{r}'}\hat{\eta}_{\mathbf{r}'}\hat{\eta}_{\mathbf{r}}\hat{b}_{\mathbf{r}}$ with $\hat{b}^{\dagger}_{\mathbf{r}'}\hat{b}_{\mathbf{r}}$ (and allowing the chemical potential to vary in space), we arrive at the Hamiltonian of Eq. (1). Considering a typical experimental setup [25], we obtain $U \sim 0.1\epsilon_b$, $t/U \sim 0.1$–10% in the range of optical lattice depth being 12–$3E_R$, and $V/U \sim 10$ (regime of the wedding-cake structure of even-filling MIs), where ϵ_b is the binding energy of a pair of fermions and E_R is the recoil energy. One can also expect a high tunability of U and V via the tuning of the Feshbach-resonant [87] interactions and the overall trapping potential used in the experiments.

[1] J. Hubbard, Proc. R. Soc. A **276**, 238 (1963).
[2] D. Belitz and T. R. Kirkpatrick, Rev. Mod. Phys. **66**, 261 (1994).
[3] E. Dagotto, Rev. Mod. Phys. **66**, 763 (1994).
[4] M. Imada, A. Fujimori, and Y. Tokura, Rev. Mod. Phys. **70**, 1039 (1998).
[5] P. A. Lee, N. Nagaosa, and X.-G. Wen, Rev. Mod. Phys. **78**, 17 (2006).
[6] M. P. A. Fisher, P. B. Weichman, G. Grinstein, and D. S. Fisher, Phys. Rev. B **40**, 546 (1989).
[7] S. Sachdev, *Quantum Phase Transitions* (Cambridge University Press, Cambridge, England, 1999).
[8] H. S. J. van der Zant, F. C. Fritschy, W. J. Elion, L. J. Geerligs, and J. E. Mooij, Phys. Rev. Lett. **69**, 2971 (1992).
[9] A. van Oudenaarden and J. E. Mooij, Phys. Rev. Lett. **76**, 4947 (1996).
[10] R. M. Dimeo, P. E. Sokol, C. R. Anderson, W. G. Stirling, K. H. Andersen, and M. A. Adams, Phys. Rev. Lett. **81**, 5860 (1998).
[11] O. Plantevin, B. Fåk, H. R. Glyde, N. Mulders, J. Bossy, G. Coddens, and H. Schober, Phys. Rev. B **63**, 224508 (2001).
[12] D. Jaksch, C. Bruder, J. I. Cirac, C. W. Gardiner, and P. Zoller, Phys. Rev. Lett. **81**, 3108 (1998).
[13] M. J. Hartmann, F. G. S. L. Brandão, and M. B. Plenio, Nat. Phys. **2**, 849 (2006).
[14] A. D. Greentree, C. Tahan, J. H. Cole, and L. C. L. Hollenberg, Nat. Phys. **2**, 856 (2006).
[15] C. W. Lai, N. Y. Kim, S. Utsunomiya, G. Roumpos, H. Deng, M. D. Fraser, T. Byrnes, P. Recher, N. Kumada, T. Fujisawa, and Y. Yamamoto, Nature (London) **450**, 529 (2007).
[16] T. Byrnes, P. Recher, and Y. Yamamoto, Phys. Rev. B **81**, 205312 (2010).
[17] M. Greiner, O. Mandel, T. Esslinger, T. W. Hansch, and I. Bloch, Nature (London) **415**, 39 (2002).
[18] G. K. Campbell, J. Mun, M. Boyd, P. Medley, A. E. Leanhardt, L. G. Marcassa, D. E. Pritchard, and W. Ketterle, Science **313**, 649 (2006).
[19] D. Jaksch and P. Zoller, Ann. Phys. **315**, 52 (2005).
[20] O. Morsch and M. Oberthaler, Rev. Mod. Phys. **78**, 179 (2006).

[21] I. Bloch, J. Dalibard, and W. Zwerger, Rev. Mod. Phys. **80**, 885 (2008).

[22] M. A. Cazalilla, R. Citro, T. Giamarchi, E. Orignac, and M. Rigol, Rev. Mod. Phys. **83**, 1405 (2011).

[23] N. Marzari, A. A. Mostofi, J. R. Yates, I. Souza, and D. Vanderbilt, Rev. Mod. Phys. **84**, 1419 (2012).

[24] K. Sun and C. J. Bolech, Phys. Rev. A **85**, 051607(R) (2012).

[25] Y. Liao, A. S. C. Rittner, T. Paprotta, W. Li, G. B. Partrige, R. G. Hulet, S. K. Baur, and E. J. Mueller, Nature (London) **467**, 567 (2010).

[26] P. Fulde and R. A. Ferrell, Phys. Rev. **135**, A550 (1964).

[27] A. I. Larkin and Yu. N. Ovchinnikov, Sov. Phys. JETP **20**, 762 (1965) [Zh. Eksp. Teor. Fiz. **47**, 1136 (1964)].

[28] S. Giorgini, L. P. Pitaevskii, and S. Stringari, Rev. Mod. Phys. **80**, 1215 (2008).

[29] L. Radzihovsky and D. E. Sheehy, Rep. Prog. Phys. **73**, 076501 (2010).

[30] F. Alet, S. Wessel, and M. Troyer, Phys. Rev. E **71**, 036706 (2005).

[31] F. Alet, P. Dayal, A. Grzesik, M. Honecker, A. Laeuchli, S. R. Manmana, I. P. McCulloch, F. Michel, R. M. Noack, G. Schmid *et al.*, J. Phys. Soc. Jpn. **74**, 30 (2005).

[32] A. F. Albuquerque *et al.*, J. Magn. Magn. Mater. **310**, 1187 (2007).

[33] B. Bauer *et al.*, J. Stat. Mech. (2011) P05001.

[34] D. S. Rokhsar and B. G. Kotliar, Phys. Rev. B **44**, 10328 (1991).

[35] C. Trefzger, C. Menotti, and M. Lewenstein, Phys. Rev. Lett. **103**, 035304 (2009).

[36] A. Hu, L. Mathey, I. Danshita, E. Tiesinga, C. J. Williams, and C. W. Clark, Phys. Rev. A **80**, 023619 (2009).

[37] C. Menotti and S. Stringari, Phys. Rev. A **81**, 045604 (2010).

[38] S. Diehl, M. Baranov, A. J. Daley, and P. Zoller, Phys. Rev. Lett. **104**, 165301 (2010); Phys. Rev. B **82**, 064509 (2010); **82**, 064510 (2010).

[39] L. Bonnes and S. Wessel, Phys. Rev. Lett. **106**, 185302 (2011).

[40] K.-K. Ng and M.-F. Yang, Phys. Rev. B **83**, 100511(R) (2011).

[41] Y.-C. Chen, K.-K. Ng, and M.-F. Yang, Phys. Rev. B **84**, 092503 (2011).

[42] H. Moritz, T. Stöferle, K. Güenter, M. Köhl, and T. Esslinger, Phys. Rev. Lett. **94**, 210401 (2005).

[43] M. Aidelsburger, M. Atala, S. Nascimbène, S. Trotzky, Y.-A. Chen, and I. Bloch, Phys. Rev. Lett. **107**, 255301 (2011).

[44] E. Altman and A. Auerbach, Phys. Rev. Lett. **89**, 250404 (2002).

[45] M. N. Barber and M. T. Batchelor, Phys. Rev. B **40**, 4621 (1989).

[46] G. Fáth and J. Sólyom, Phys. Rev. B **44**, 11836 (1991); **47**, 872 (1993); **51**, 3620 (1995).

[47] B. A. Ivanov and A. K. Kolezhuk, Phys. Rev. B **68**, 052401 (2003).

[48] Ö. Legeza and J. Sólyom, Phys. Rev. Lett. **96**, 116401 (2006).

[49] A. Läuchli, G. Schmid, and S. Trebst, Phys. Rev. B **74**, 144426 (2006).

[50] Z.-X. Liu, Yi Zhou, H.-H. Tu, X.-G. Wen, and T.-K. Ng, Phys. Rev. B **85**, 195144 (2012).

[51] Y. A. Fridman, O. A. Kosmacheva, and P. N. Klevetsa, J. Magn. Magn. Mater. **325**, 125 (2013).

[52] H. Tsunetsugu and M. Arikawa, J. Phys. Soc. Jpn. **75**, 083701 (2006).

[53] S. K. Yip, Phys. Rev. Lett. **90**, 250402 (2003).

[54] J. J. Garcià-Ripoll, M. A. Martin-Delgado, and J. I. Cirac, Phys. Rev. Lett. **93**, 250405 (2004).

[55] F. D. M. Haldane, Phys. Lett. A **93**, 464 (1983); Phys. Rev. Lett. **50**, 1153 (1983).

[56] H. Kadowaki, K. Ubukoshi, and K. Hirakawa, J. Phys. Soc. Jpn. **56**, 751 (1987).

[57] I. Affleck, J. Phys.: Condens. Matter **1**, 3047 (1989).

[58] J. P. Kestner, B. Wang, J. D. Sau, and S. Das Sarma, Phys. Rev. B **83**, 174409 (2011).

[59] B. DeMarco, C. Lannert, S. Vishveshwara, and T.-C. Wei, Phys. Rev. A **71**, 063601 (2005).

[60] O. Gygi, H. G. Katzgraber, M. Troyer, S. Wessel, and G. G. Batrouni, Phys. Rev. A **73**, 063606 (2006); C. Kollath, A. M. Läuchli, and E. Altman, Phys. Rev. Lett. **98**, 180601 (2007); S. Wessel, Phys. Rev. B **75**, 174301 (2007); Comput. Phys. Commun. **177**, 166 (2007); Phys. Rev. B **78**, 075112 (2008); S. Guertler, M. Troyer, and F.-C. Zhang, *ibid.* **77**, 184505 (2008); K. P. Schmidt, Julien Dorier, and Andreas M. Läuchli, Phys. Rev. Lett. **101**, 150405 (2008); K. Yamamoto, S. Todo, and S. Miyashita, Phys. Rev. B **79**, 094503 (2009); A. Kalz, A. Honecker, S. Fuchs, and T. Pruschke, *ibid.* **83**, 174519 (2011); E. Arrigoni, M. Knap, and W. von der Linden, *ibid.* **84**, 014535 (2011).

[61] A. Albus, F. Illuminati, and J. Eisert, Phys. Rev. A **68**, 023606 (2003); L. Pollet, S. Rombouts, K. Heyde, and J. Dukelsky, *ibid.* **69**, 043601 (2004); T. Kimura, S. Tsuchiya, and S. Kurihara, Phys. Rev. Lett. **94**, 110403 (2005); V. W. Scarola and S. Das Sarma, *ibid.* **95**, 033003 (2005); V. W. Scarola and S. Das Sarma, *ibid.* **98**, 210403 (2007); T. Miyakawa and P. Meystre, Phys. Rev. A **74**, 043615 (2006); P. Buonsante, F. Massel, V. Penna, and A. Vezzani, *ibid.* **79**, 013623 (2009); M. Yamashita and M. W. Jack, *ibid.* **79**, 023609 (2009); K. Sun, C. Lannert, and S. Vishveshwara, *ibid.* **79**, 043422 (2009); M. Iskin, *ibid.* **83**, 051606 (2011); T. Kimura, *ibid.* **84**, 063630 (2011); T. Saito, I. Danshita, T. Ozaki, and T. Nikuni, *ibid.* **86**, 023623 (2012); D. Pekker, B. Wunsch, T. Kitagawa, E. Manousakis, A. S. Sorensen, and E. Demler, Phys. Rev. B **86**, 144527 (2012); C.-H. Lin, R. Sensarma, K. Sengupta, and S. Das Sarma, *ibid.* **86**, 214207 (2012); D.-S. Lühmann, Phys. Rev. A **87**, 043619 (2013); M. Yamashita, S. Kato, A. Yamaguchi, S. Sugawa, T. Fukuhara, S. Uetake, and Y. Takahashi, *ibid.* **87**, 041604 (2013); P. Buonsante, L. Orefice, and A. Smerzi, *ibid.* **87**, 063620 (2013).

[62] R. Hulet and his group (private communication).

[63] T. Stöferle, H. Moritz, C. Schori, M. Köhl, and T. Esslinger, Phys. Rev. Lett. **92**, 130403 (2004).

[64] R. Jördens, N. Strohmaier, K. Günter, H. Moritz, and T. Esslinger, Nature (London) **455**, 204 (2008).

[65] T. Kinoshita, T. Wenger, and D. S. Weiss, Science **305**, 1125 (2004); Nature (London) **440**, 900 (2006).

[66] M. Swanson, Y. L. Loh, and N. Trivedi, New J. Phys. **14**, 033036 (2012).

[67] Hong Lu, L. O. Baksmaty, C. J. Bolech, and Han Pu, Phys. Rev. Lett. **108**, 225302 (2012).

[68] C. J. Bolech, F. Heidrich-Meisner, S. Langer, I. P. McCulloch, G. Orso, and M. Rigol, Phys. Rev. Lett. **109**, 110602 (2012).

[69] K. Sun and C. J. Bolech, Phys. Rev. A **87**, 053622 (2013).

[70] P. G. de Gennes, *Superconductivity of Metals and Alloys* (Addison-Wesley, Reading, MA, 1989).

[71] T. Mizushima, K. Machida, and M. Ichioka, Phys. Rev. Lett. **94**, 060404 (2005).
[72] M. M. Parish, S. K. Baur, E. J. Mueller, and D. A. Huse, Phys. Rev. Lett. **99**, 250403 (2007).
[73] X.- Ji Liu, H. Hu, and P. D. Drummond, Phys. Rev. A **76**, 043605 (2007); **78**, 023601 (2008).
[74] L. O. Baksmaty, H. Lu, C. J. Bolech, and H. Pu, Phys. Rev. A **83**, 023604 (2011); New J. Phys. **13**, 055014 (2011).
[75] K. Sun, J. S. Meyer, D. E. Sheehy, and S. Vishveshwara, Phys. Rev. A **83**, 033608 (2011).
[76] N. Yoshida and S.-K. Yip, Phys. Rev. A **75**, 063601 (2007).
[77] S. Brazovskii, Physica B **404**, 482 (2009).
[78] R. M. Lutchyn, M. Dzero, and V. M. Yakovenko, Phys. Rev. A **84**, 033609 (2011).
[79] Y. L. Loh and N. Trivedi, Phys. Rev. Lett. **104**, 165302 (2010).
[80] D.-H. Kim and P. Törmä, Phys. Rev. B **85**, 180508 (2012).
[81] G. Wirth, M. Ölschläger, and A. Hemmerich, Nat. Phys. **7**, 147 (2011).
[82] X. Li, E. Zhao, and W. V. Liu, Nat. Commun. **4**, 1523 (2013).
[83] M. Ölschläger, T. Kock, G. Wirth, A. Ewerbeck, C. Morais Smith, and A. Hemmerich, New J. Phys. **15**, 083041 (2013).
[84] F. Hébert, Zi Cai, V. G. Rousseau, C. Wu, R. T. Scalettar, and G. G. Batrouni, Phys. Rev. B **87**, 224505 (2013).
[85] X. Li, A. Paramekanti, A. Hemmerich, and W. V. Liu, Nat. Commun. **5**, 3205 (2014).
[86] A. I. Buzdin, Rev. Mod. Phys. **77**, 935 (2005).
[87] C. Chin, R. Grimm, P. Julienne, and E. Tiesinga, Rev. Mod. Phys. **82**, 1225 (2010).